Full Title: **Phase-specific premotor inhibition modulates leech rhythmic motor output**

Martina Radice[1,2], Agustín Sanchez Merlinsky[1], Federico Yulita[1,3] and Lidia Szczupak[1,2]

1 Instituto de Fisiología, Biología Molecular y Neurociencias (IFIBYNE-UBA-CONICET), Buenos Aires, Argentina

2 Departamento de Fisiología, Biología Molecular y Celular, Facultad de Ciencias Exactas y Naturales, Universidad de Buenos Aires, Buenos Aires, Argentina

3 Departamento de Física, Facultad de Ciencias Exactas y Naturales, Universidad de Buenos Aires, Buenos Aires, Argentina

Corresponding Author: Lidia Szczupak, lidiaszczupak@gmail.com

ABSTRACT

Understanding how motoneuron activity is finely tuned remains an open question. Leeches are a highly suitable organism for studying motor control due to their well-characterized behaviors and relatively simple nervous system. On solid surfaces leeches display crawling, a rhythmic motor pattern that can be elicited in the isolated nerve cord or even in single ganglia isolated from it. This study aimed to learn how this motor output is shaped by concurrent premotor signals. Specifically, we analyzed how electrophysiological manipulation of a premotor nonspiking (NS) neuron, that forms a recurrent inhibitory circuit (homologous to vertebrate Renshaw cells), shapes the leech crawling motor pattern. The study included a quantitative analysis of motor units active throughout the fictive crawling cycle that shows that the rhythmic motor output in isolated ganglia mirrors the phase relationships observed *in vivo*. Taken together, the study reveals that the premotor NS neurons, under the control of the segmental pattern generator, modulated the degree of excitation of motoneurons during crawling in a phase-specific manner.

INTRODUCTION

Animal locomotion involves the coordination of multiple muscles under the control of the nervous system. To ensure smooth movements, diverse regulatory mechanisms operate at different hierarchical levels within the motor system, narrowing down the degrees of freedom of a highly distributed system with multiple units. The overall functional organization and operational logic of motor systems, comprising the components at all levels of the hierarchy and their feedforward and feedback interactions, remain, to a great extent, an open question in both vertebrates and invertebrates (Kiehn, 2016; Arber and Costa, 2018; Barkan and Zornik, 2019; Grätsch et al., 2019); this includes the mechanisms that operate at the level of the nerve cord (Grillner and El Manira, 2020; McLean and Dougherty, 2015; Gal, 2017; Sengupta and Bagnall, 2023; Calabrese and Marder, 2024). Analysis of this organization across different organisms, developmental stages, and behavioral repertoires has provided fruitful information. Leeches have been highly useful to study motor control due to their robust repertoire of motor behaviors, which are executed by a relatively simple body plan and controlled by a similarly simple nervous system. This system is composed of a chain of 21 midbody ganglia flanked by head and tail brains (Wagenaar, 2015), where each midbody ganglion contains the sensory and motor neurons that innervate the corresponding segment (Muller et al., 1981).

On solid surfaces, leeches exhibit a robust rhythmic motor pattern known as crawling (Figure 1A). This behavior results from waves of elongation and contraction of the body along its antero-posterior axis, as the animal is anchored on the posterior and anterior suckers, respectively (Stern-Tomlinson et al., 1986, Figure 1A). Fictive crawling (*crawling*) can be monitored in the isolated nervous system, where identified interneurons and motoneurons can be recorded intracellularly and extracellularly (Baader, 1997; Baader and Kristan, 1992; Eisenhart

et al., 2000). The pattern is characterized by the alternating activation of the motoneurons, such as CV and DE-3, that innervate circular and longitudinal muscles, respectively (Figure 1B). This pattern can be readily evoked by dopamine in the isolated nerve cords (Puhl and Mesce, 2008), in short chains of ganglia (Kearney et al., 2022), and in single isolated ganglia (Puhl and Mesce, 2008; Rodriguez et al., 2012). These studies established that each ganglion contains the network responsible for producing the rhythmic motoneuron activity compatible with crawling. Note that in the context of this manuscript fictive crawling refers to the rhythm generation but does not include the connectivity that rules intersegmental interactions and the consequent intersegmental lags.

Studies on motor behaviors in diverse organisms show that, at the final stage of neural processing, motoneuron activity is controlled by multiple signal sources (El Manira, 2023; Zhen and Samuel, 2015; Rotstein et al., 2017). Analysis of the nature and effects of these signals on the motor pattern is an active field of research. The present work has focused on the role played by nonspiking (NS) premotor neurons on leech crawling. These neurons are present as bilateral pairs in each segmental ganglion and are functional homologs of the mammalian Renshaw cells (Szczupak, 2014). These spinal cord cells receive excitatory inputs from motoneurons and, in turn, transmit inhibitory signals to the motoneurons (Alvarez and Fyffe, 2007).

Each pair of NS neurons is at the center of a recurrent inhibitory circuit mediated by chemical and electrical synaptic connections with the motoneurons (Figure 1C) (Rela and Szczupak, 2003; Rodriguez et al., 2009). In the context of this circuit the activity of excitatory motoneurons evokes chemically mediated inhibitory synaptic potentials in NS. Additionally, the NS neurons are electrically coupled to virtually all excitatory motoneurons via rectifying junctions that conduct when the transjunction NS-motoneuron potential is negative. In

72 physiological conditions this coupling favors the transmission of inhibitory signals from NS to
73 motoneurons. Given this recurrent inhibitory circuit, NS premotor neurons could operate as
74 modulators of motoneuron activity. A previous study (Rodriguez et al., 2012) indicated that NS
75 membrane potential oscillates in tune with the *crawling* motor pattern and that this premotor
76 neuron can indeed modulate motor activity. In that study *crawling* was monitored by the
77 recording of a particular motoneuron, the dorsal excitor cell 3 (DE-3). However, the wide
78 connectivity of NS with several excitatory motoneurons that fire during *crawling*, called for a
79 more comprehensive readout of the motor pattern.

80 The present study aimed to evaluate the influence of the premotor NS neuron along the
81 different stages of *crawling*. For this purpose, we describe the pattern of activity of different
82 neurons during *crawling* which were simultaneously monitored through extracellular nerve
83 recordings while manipulating the NS membrane potential. The study reveals that the premotor
84 neuron mediated a reduction of the firing frequency of motoneurons recruited during a specific
85 phase of *crawling*.

RESULTS

NS membrane potential oscillations during *crawling*

To study the role that premotor NS neurons play in fictive crawling (*crawling)* we first analyzed the correspondence between NS electrophysiological activity and the motoneuron output during this motor pattern. Since motoneuron DE-3 (dorsal excitor cell 3), which innervates the longitudinal dorsal muscle fibers, is the most robust proxy of *crawling* (Puhl and Mesce, 2008), extracellular recordings of this motoneuron in the DP nerve were combined with NS intracellular recordings. As shown previously (Rodriguez et al., 2012), the NS membrane potential showed rhythmic oscillations tuned to DE-3 activity, with hyperpolarizations occurring in conjunction with DE-3 bursts and depolarizations during DE-3 silent phases (Figure 2A). Here, a cross-correlation analysis between NS and DE-3 firing frequency revealed a marked anticorrelation, with a cross-correlation index of -0.61 ± 0.03 (mean ± SEM) at a lag close to 0 sec (0.24 ± 0.10 s) (Figure 2B). This result indicates that NS hyperpolarization takes place in phase with DE-3 bursts.

In the frame of the recurrent inhibitory circuit, NS is the target of inhibitory signals evoked by excitatory motoneurons via chemically-mediated polysynaptic pathways (Rela and Szczupak, 2003, Figure 1C). Thus, it was hypothesized that the NS hyperpolarizations observed during *crawling* resulted from inputs originating in DE-3 and other motoneurons that fire in phase with it (Rodriguez et al., 2012). If this hypothesis was correct, the onset of DE-3 bursts should precede the onset of NS hyperpolarization. Because the cross-correlation was performed on binned DE-3 firing frequency curves, the peak lag reported does not offer a proper estimation of the relative timing between the two signals. To gain a more precise assessment, NS intracellular recordings were segmented into individual cycles and aligned with the first spike of

109 the corresponding DE-3 burst (Figure 2C). As shown in the figure, because of the NS membrane
110 potential oscillations it is not possible to establish a sharp onset for the NS hyperpolarizing
111 response. However, the example illustrates that the onset of the DE-3 bursts occurred after NS
112 hyperpolarization was already initiated. These findings rule out the possibility that the NS
113 hyperpolarization was originated by DE-3 bursting. Instead, they suggest that NS and DE-3
114 received concomitant rhythmic inputs of opposite sign—that is, hyperpolarizing inputs in NS and
115 depolarizing ones in DE-3.

116 To further analyze the putative concomitant inputs from the pattern generator onto NS
117 and DE-3, we evaluated the correlation between different features of their rhythmic activity
118 (Figure 2A). We found no relationship between the amplitude of NS hyperpolarization and DE-3
119 mean firing frequency (Figure 2D). However, surprisingly, the former exhibited a high
120 correlation with DE-3 burst duration (Figure 2E). This result led to examining how the amplitude
121 of NS hyperpolarization related to the time between consecutive DE-3 bursts (interbursts time),
122 preceding (pre) and following (post) the NS hyperpolarization (Figure 2A). The data show a
123 significant correlation of the amplitude of NS hyperpolarization with the pre-interburst duration,
124 but not with the post-interburst duration (Figure 2F-G). Taken in consideration the putative
125 model presented in Figure 1C, in which the oscillator units C and E inhibit each other, the longer
126 the activity of unit E, the larger the rebound in unit C and its downstream effects on NS
127 hyperpolarization and on DE-3 burst duration.

128 These results indicate that, in addition to the known recurrent inhibitory circuit between
129 NS and motoneurons, NS neurons receive an inhibitory signal during *crawling*, which is in phase
130 with DE-3 activity. This inhibitory signal seems to have originated from the same source that
131 activates DE-3 motoneurons. In that case, it seems puzzling to find a lack of correlation between

132 NS hyperpolarization amplitude and DE-3 firing frequency. However, this observation might be
133 explained by considering that DE-3 is subjected to two counteracting effects at the same time: an
134 excitatory input from the oscillator unit C and an inhibitory input from NS via the rectifying
135 electrical junctions (Figure 1C).
136
137 **Effect of NS on DE-3 activity during *crawling***
138 In a previous study (Rodriguez et al., 2012) we showed that hyperpolarization of NS during
139 *crawling* reduced the firing frequency of DE-3, suggesting that the premotor neuron preserved
140 the influence that exhibits in basal conditions during the rhythmic motor pattern (Rodriguez et
141 al., 2009). Here we aimed at testing whether the inhibitory signal that NS receives during
142 crawling is indeed transmitted to the motoneurons. For this purpose the premotor neuron was
143 transiently removed from the circuit. In line with the properties of the rectifying electrical
144 synapse between NS and the motoneurons, depolarizing NS neurons is equivalent to
145 disconnecting them from the network (Rela and Szczupak, 2007). The work by Rodriguez et al.
146 (2012) showed that NS depolarization increased DE-3 firing frequency but the study lacked
147 appropriate controls that we carried out here.
148 Depolarizing steps applied in NS neurons in the course of *crawling* episodes (Figure 3A)
149 shifted their membrane potential beyond +100 mV, well above the average membrane potential
150 of the motoneurons. An important control introduced here evaluate potential drifts in *crawling*
151 features over time. For this purpose we compared two series of experiments: one in which NS
152 was subjected to depolarizing steps (depo) and a control (ctrl) in which it was not. We assessed
153 changes in cycle period, DE-3 mean firing frequency (mFF), burst duration and duty cycle for
154 both treatments (depo, ctrl) across different epochs (pre, test, post).

155 Transient NS depolarizations had no effect on the *crawling* period (measured in end-to-
156 end cycles, see Materials and Methods), DE-3 burst duration and duty cycle (Figure 3B), but
157 produced a 60% increase in DE-3 mFF (Figure 3B-C).
158 In the control series the analysis of *crawling* features over time shows that cycle period
159 and DE-3 burst duration decreased over epochs, while the duty cycle remained constant. Similar
160 results were obtained when cycles were segmented from start-to-start (data not shown). Thus,
161 throughout the dopamine perfusion the motor pattern exhibited an acceleration but the duty cycle
162 remained stable.
163 This series of experiments proves that, as predicted based on the known circuit (Figure
164 1C), inhibitory signals onto NS premotor neurons were transmitted to DE-3 motoneurons and
165 counteracted their excitatory drive during *crawling*, limiting their firing frequency.
166
167 **A more comprehensive view of *crawling***
168 As indicated above, the activity of motoneuron DE-3 has been widely used as a proxy of
169 *crawling*. However, focusing on a single motoneuron neglects possible effects of NS on other
170 phases of the motor pattern. To evaluate whether the effect of the premotor NS neuron extends to
171 other motoneurons active during *crawling*, we performed extracellular recordings of DP along
172 with AA and/or PP root nerves. Single units were identified using a spike sorting algorithm
173 (Figure 4Ai-Aii) that enabled a systematic analysis of their activity. The firing pattern of
174 detected units (Figure 4Aiii) was expressed as binned firing frequency (bFF). Because DE-3 is
175 used as a reference marker of the cycle, segmentation of the traces was performed using the start-
176 to-start approach (see Material and Methods). This rhythmic activity shows that some units fire

177 during the contraction stage, defined by DE-3 activity, while others fire during the elongation
178 phase.

179 Plotting the bFF of the different rhythmic units as a function of phase within a *crawling*
180 cycle (start-to-start) allowed for the manual classification of the unit. Based on their activity
181 profile relative to DE-3 three types were identified: In-Phase, Anti-Phase, or In-Phase-Early-
182 Onset (Figure 4B). The In-phase units fire simultaneously with DE-3, the Anti-Phase units fire in
183 between DE-3 bursts, and the In-Phase-Early-Onset units are active in phase with DE-3 but start
184 firing before DE-3 burst onset (Figure 4C).

185 Multiple intracellular recordings represent a challenge, and therefore recording the
186 activity of different motoneurons during crawling has been restricted to one (Puhl and Mesce,
187 2008) or two (Rodriguez et al., 2012) cells at a time. While multiple extracellular recordings
188 have been performed previously (Eisenhart et al., 2000), these results (Figure 4) present the first
189 quantitative analysis of motor units activated throughout the *crawling* cycle in this type of
190 recordings. The In-Phase units are expected to control the contraction stage by exciting or
191 inhibiting the longitudinal or circular muscles, respectively, and the Anti-Phase units to control
192 the elongation stage by exciting or inhibiting the circular or longitudinal muscles, respectively. It
193 is plausible that In-Phase-Early-Onset are inhibitors of circular muscles, preparing the conditions
194 for a fast contraction stage. Further studies should confirm this hypothesis.

195

196 **Comparison of the motor pattern in single ganglia and in intact animals**

197 The assumption that the crawling motor pattern described on the basis of extracellular recordings
198 in isolated single ganglia, reflects key characteristics of the behavioral pattern, requires
199 qualitative and quantitative validation. To this end intact leeches were monitored during

200 crawling. The analysis was performed by tracking nine dots painted along the dorsal longitudinal
201 midline of the leech, which divided the body into 8 sections (Figure 5A). Because ganglia are
202 located in highly conserved positions relative to the length of the animal (Figure 5B, Kearney et
203 al. 2022), the relative distance from the head can be used to infer which ganglia are included
204 within the 8 sections mentioned above. We focused the analysis on sections delimited by points
205 4-5 and 5-6, that correspond to the range of segmental ganglia included in the *ex vivo* studies
206 (ganglia 8 to 15) (Figure 5A-B). For electrophysiological data the frame of analysis was the
207 cycle of DE-3 rhythmic activity and, equivalently, for the behavioral data the frame of analysis
208 was the crawling step (see Materials and Methods).

209 Figure 5C shows a representative trace of a series of whole length waves, that were
210 divided into discrete steps (see Materials and Methods), and the corresponding measurements in
211 the section delimited by the dots 4 and 5. Within each crawling step, four stages were identified
212 in the studied sections (Figure 5C): the elongation stage (marked by an increase in section
213 length), the contraction stage (marked by a decrease in section length) and two isometric stages
214 flanking the dynamic stages. The plot in Figure 5D shows the section length of different steps by
215 the same animal, normalized by the step duration, and illustrates the variability of the step
216 dynamics.

217 For a quantitative comparison of the *in vivo* and *ex vivo* experiments the following
218 variables were evaluated: period of the rhythmic pattern and duty cycle of the different phases.
219 While the average cycle period (end-to-end) recorded in isolated ganglia was of 15.22 ± 3.21 s (n
220 = 6), the average duration of the leech step was of 7.49 ± 0.50 s (n=6). These values are similar
221 to those reported in previous studies (Puhl and Mesce, 2008, for single ganglia; and Stern-
222 Tomlinson et al., 1986; Baader and Kristan, 1992 and Puhl and Mesce, 2008, for intact animals).

223 Thus, in the intact animal the rhythmic activity was twice as fast as in the isolated ganglion,
224 suggesting that peripheral signals may accelerate the rhythmic behavior, as already described in
225 other animals (Pulver et al., 2015; Fushiki et al., 2016). However, we cannot rule out that
226 activation of the rhythmogenic circuit in isolated ganglia may fail to activate a circuit component
227 responsible for speeding the rhythm.

228 It seems natural to correlate the activity of the Anti-Phase and In-Phase units of *ex vivo*
229 studies with the elongation and contraction stages of *in vivo* behavior, respectively. But the
230 isometric stages displayed *in vivo* at the section level have no obvious counterpart in the
231 electrophysiological recordings of motoneurons in the isolated ganglia. It is important to
232 consider that the rhythmic movement of successive segments along the antero-posterior axis of
233 the animal requires a delay signal that allows the appropriate propagation of the metachronal
234 wave (Puhl and Mesce, 2010; Puhl et al 2012), and this signal is probably absent in the isolated
235 ganglion. In consequence, for the comparison of the duty cycle, the *in vivo* isometric stages were
236 ignored, and only the duration of the dynamic fraction of the step was taken in consideration. In
237 turn, the behavioral duty cycle was calculated as the ratio between the elongation or contraction
238 stage duration over the dynamic step duration. Thus measured, the duty cycle of the elongation
239 stage was 0.65 ± 0.01 and that of the contraction was 0.35 ± 0.01 (Figure 5E). These values are
240 noticeably close to the duty cycle of the Anti-Phase units (0.64 ± 0.07) and of the DE-3
241 motoneurons (0.32 ± 0.03) (Figure 5E) measured in the isolated ganglia.

242 These results show that the dynamic pattern described by multiple motoneurons recorded
243 in isolated ganglia reflects the phase relation observed in the corresponding body section *in vivo*.
244

245 **Effect of NS on the activity of the different types of motoneurons during *crawling***

246 The results shown in Figure 5 support the view that the activity recorded in single isolated
247 ganglia reflects the neuronal control of the rhythmic motor pattern underlying crawling. Based
248 on this premise the recording of multiple units presented above was used to evaluate the
249 influence of NS on units active at different *crawling* stages (Figure 6Ai-ii). Previous work
250 (Rodriguez et al., 2012) and the experiments presented in Figure 3 suggest that NS
251 depolarization releases motoneuron DE-3 from the inhibitory influence of the premotor neuron.
252 The suggested interpretation postulates that NS depolarization, by turning off the rectifying
253 junctions, prevents the transmission of NS inhibitory inputs onto DE-3. Given the widespread
254 connectivity of NS with all the excitatory motoneurons, it is expected that NS manipulation
255 affects the activity of all the units that fire in phase with DE-3 when NS receives inhibitory
256 inputs (Figure 2A). In contrast, units active in anti-phase with DE-3 should not be affected as NS
257 does not receive inhibitory inputs during that stage.

258 To evaluate the effect of NS depolarization, the activity of the motoneurons was
259 characterized using two metrics: maximum bFF (Max bFF) to assess activity level, and relative
260 half width (Rel HW) to evaluate the duty cycle. To enable a comparison with the other units, the
261 data for DE-3 was reanalyzed in this manner.

262 NS depolarization produced an increase in DE-3 Max bFF of around 60% (as shown
263 above), while this variable remained stable throughout control experiments (Figure 6B).
264 Different from DE-3, In-Phase units showed a marked decrease in the maximum bFF along time
265 in control conditions, but similar to DE-3, this variable underwent an increase of around 50%
266 upon NS depolarization (Figure 6B). Given the temporal drop detected in the control series this
267 increase is probably an underestimation of the NS effect on the In-Phase firing frequency.

268 The Anti-Phase units also showed a slight but significant decrease in the maximum bFF
269 along time in control conditions, but in this case the effect of NS depolarization was limited to
270 counteracting this decrease (Figure 6B). While in control conditions Anti-Phase motor units
271 exhibited a decrease of around 15% between pre and test epochs, the depo experiments showed
272 no decrement between these two epochs. Notwithstanding, control and depo experiments showed
273 a marked decrease in bFF from test to post (15% and a 20% decrease, respectively). NS
274 depolarization did not affect the maximum bFF of the In-Phase-Early-Onset units (Figure 6B).
275 Regarding the relative HW, the effect of NS depolarization was limited to In-Phase units.
276 Our results show that the relative HW of these units tended to fall along epochs in control
277 conditions and that releasing NS depolarization enhanced this tendency (Figure 6C). In control
278 experiments, the relative HW decreased by about 15% between test and post epochs; and in the
279 depo experiments the decrease was of around 40%.
280 The statistical analyses, as well as the estimated ratios between epochs for each case, are
281 detailed in Supplementary Table 2.
282 Taken together, the results support the hypothesis presented earlier: the inhibitory signals
283 received by NS in phase with the contraction stage modulated the activity of the motoneurons
284 active in this instance. It is worth noting that the fact that the firing frequency of Anti-Phase MNs
285 was not affected by NS depolarization indicates that this experimental manipulation did not
286 cause a generalized change in the activity of MNs.

287 **DISCUSSION**

288 The present study shows that phase specific inhibitory signals, delivered by the functional
289 homolog of Renshaw cells in the leech (Szczupak, 2014), modulate the degree of excitation of
290 the motoneurons responsible for the contraction stage of *crawling*. This effect was phase
291 specific, as motoneurons active in the rest of the cycle were not affected. NS is a premotor
292 neuron that operates at the center of a recurrent inhibitory circuit (Rela and Szczupak, 2003;
293 Rodriguez et al., 2009) and thus the initial hypothesis suggested that the effect on *crawling* was
294 mediated entirely by this circuit. However, the results show that the inhibitory signal did not
295 originate at the level of the motoneurons themselves but, most probably, at the crawling
296 oscillator. The marked temporal correlation between the neurons active at the contraction stage
297 and NS hyperpolarizations suggests that the excitatory signals onto the motoneurons and the
298 hyperpolarizing signals onto NS were driven by the same upstream element (e.g. the element in
299 the oscillator that controls the contraction stage). This result further feeds the homology between
300 vertebrate Renshaw cells and leech NS neurons in that the formers are not only targeted by
301 motoneuron inputs but by rhythmogenic premotor elements as well (Nishimaru et al., 2006).
302 Nonetheless, the results do not rule out that the existing recurrent inhibitory circuit contributes to
303 the hyperpolarization of NS.

304 On the other hand, the fact that In-Phase-Early-Onset activity was also unaffected by NS
305 depolarization confirms that these motoneurons constitute a distinct group from the In-Phase
306 units. Furthermore, this suggests that these units might be inhibitory motoneurons that are not
307 connected to the NS via the recurrent inhibitory circuit (Rela and Szczupak, 2003; Wadepuhl,
308 1989).

309 In summary, we propose that the crawling oscillator releases a dual signal onto the
310 motoneurons that control the contraction stage: a direct excitatory input that elicits the rhythmic
311 bursts and a concurrent inhibitory input via NS (Figure 7). Coherent with this interpretation, the
312 activity level of the Anti-Phase units was not influenced by these inhibitory signals.

313 The corroboration of a dual counteracting set of actions on motoneuron output calls for a
314 functional interpretation. In a characterization of the electrophysiological properties of leech
315 motoneurons it was shown that DE-3 can reach a firing frequency that exceeds 100 Hz (Perez-
316 Etchegoyen et al., 2011) while the maximal muscle tension that this motoneuron can evoke is
317 achieved at around 25 Hz (Mason and Kristan, 1982). Additionally, it is relevant to consider that
318 the population of motoneurons that activate longitudinal muscles is linked by ohmic coupling
319 that can result in mutual excitation (Fan et al., 2005; Ort et al., 1974, Ashaber et al., 2021). As a
320 result, when all the activators of longitudinal muscles are excited during the contraction stage,
321 the excitatory spread can lead to runaway motoneuron activity (Hennequin et al., 2017). An
322 inhibitory signal imposed on NS can spread to all the motoneurons simultaneously (Rela and
323 Szczupak, 2003; Rodriguez et al., 2009; Wadepuhl, 1989) and thus limit the activity of the whole
324 motoneuron population.

325 Previous work showed that leech motoneurons are subjected to a generalized inhibition
326 mediated by GABA (Baca et al., 2008) while the electrically mediated inhibition exerted by NS
327 shown here is phase-specific. The existence of concurrent excitation and inhibition has been
328 revealed in vertebrate motor networks, where it was proposed as a balancing factor (Kishore et
329 al., 2014; Parkis et al., 1999; Petersen et al., 2014). In line with the present results, experiments
330 performed in zebrafish showed that in-phase inhibition originates from a set of premotor neurons
331 that comprise the Renshaw cells (Callahan et al., 2019). Neurophysiological studies in the leech

332 offer the particular advantage of allowing electrical manipulation of individual neurons in wild-
333 type adults, where they can be readily recognized by their anatomical and electrophysiological
334 characteristics. In this sense the present study offers clear-cut evidence of the dual signal
335 motoneurons receive in the course of motor control from an identified premotor element.
336 The results further highlight the notion that knowing the connectivity among neurons is
337 not sufficient to deduce its functional operation, as the dynamical interplay among them is highly
338 relevant to understand its physiological role.
339
340 **Structure of *crawling* based on MN activity and behavior**
341 Evaluation of phase specificity required a more comprehensive tracking of motoneuron activity
342 throughout the cycle and we addressed this demand through the analysis of the activity of
343 multiple motoneurons. In the present study we show that in the course of *crawling* DE-3 neurons
344 fire concurrently with neurons that reach the periphery mainly through the PP and the AA roots.
345 Based on the classical description of Ort and collaborators (1974) the spikes in phase with DE-3
346 recorded in the PP root are likely to correspond to VE-4 (ventral-excitor 4), DE-5, DE-7 and VE-
347 8, while those recorded in AA are likely to correspond to DE-107 and VE-108. Intracellular
348 recordings of VE-4, VE-5 showed indeed the coincident firing with DE-3 (Baader, 1997,
349 Eisenhart et al., 2000 and Puhl and Mesce, 2008)
350 To learn how the motoneuron readout compares with the rhythmic body movements that
351 take place in crawling we presented behavioral studies that focused on the sections of the leech
352 body that match the range of ganglia used in the electrophysiological studies. The comparison
353 shows two main differences. The period of the rhythmic animal behavior was half that measured
354 in the fictive behavior at the isolated ganglia. In addition, at the behavioral level the actual

elongation-contraction gestures were flanked by isometric stages, while in dopamine-induced *crawling* studied in isolated ganglia the rhythmic activity of the motoneurons appears as the alternation between units In-Phase with DE-3 and Anti-Phase of DE-3, with no clear references for isometric phases. The absence of known descending brain signals (Puhl et al., 2012) and/or peripheral signals are assumed as important factors in determining the cycle period and the sequence at which the different behavioral stages take place. However, it is noteworthy that taking the isometric stages aside, the sequence of events, and the proportion of the active cycle dedicated to elongation and contraction were remarkably similar in both experimental settings. This suggests that the network activated in the isolated ganglion is the one underlying the dynamic aspects of the motor behavior at any given section of the animal.

365 **MATERIALS AND METHODS**

366 **Biological Preparation**

367 Leeches (*Hirudo* sp.), weighing 1–3 g, were sourced from commercial suppliers (Niagara
368 Leeches, Cheyenne, WY, United States and Biopharm, UK) and kept at 20°C in artificial pond
369 water. These animals are hermaphrodites.

370 Studies were conducted in isolated single ganglia obtained from segments 8th to 13th.
371 The ganglia were dissected with one dorsal posterior (DP), posterior (PP) and anterior (AA)
372 nerve roots attached. The tissue was bathed in normal saline (in mM: 115 NaCl, 4 KCl, 1.8
373 $CaCl_2$, 1 $MgSO_4$, 10 Hepes, 10 glucose; pH 7.4) at room temperature (20–25°C) and pinned to
374 Sylgard (Dow Corning) in a recording chamber. The sheath covering the ganglion was dissected
375 away, exposing the neuronal cell bodies to the external solution.

376

377 **Electrophysiological Recordings**

378 Intracellular somatic recordings were conducted using microelectrodes pulled from borosilicate
379 capillary tubing (A-M Systems, Inc., Carlsborg, WA, United States), filled with 3 M potassium
380 acetate (resistance 20–40 MΩ). The electrodes were connected to an Axoclamp 2B amplifier
381 (Axon Instruments; Union City, CA, United States) operating in bridge mode. Extracellular
382 activity from DP, PP, and AA nerves was recorded using suction electrodes connected to a
383 differential a.c. amplifier (Neuroprobe 1700, A-M Systems, Inc., Carlsborg, WA, United States).
384 Intra- and extracellular recordings were digitized through an analog-digital converter (Digidata
385 1440, Axon Instruments, Union City, CA, United States) and acquired with Clampex 9.2 (Axon
386 Instruments, Union City, CA, United States) at a sampling rate of 20 kHz. Premotor NS neurons
387 were identified by their soma location and electrophysiological properties (Rela et al., 2009).

To induce fictive crawling (*crawling*), ganglia were superfused with 75 μM dopamine hydrochloride (Sigma-Aldrich, St. Louis, MO, United States), freshly prepared at the beginning of each experimental day (Puhl and Mesce, 2008). Only one episode was evoked per ganglion. The rhythmic motor pattern was monitored via extracellular recording of the DP nerve, where the largest spike corresponds to the DE-3 motoneuron, one of the motoneurons innervating the longitudinal muscles (Ort et al., 1974).

When testing the effect of NS neurons, depolarizing pulses of +5 nA to +7 nA were injected into its soma through the intracellular electrode. Between four and five *crawling* cycles before and after a depolarizing pulse were left unaffected to obtain control pre and post rhythmic epochs.

Behavioral Experiments

Leeches were anesthetized by placing individuals at −20◦C for 5 to 10 minutes. Then the skin of the animal was dried, and nine points of water-based paint were applied along its dorsal longitudinal midline (Figure 5A). When the animals recovered they were allowed to crawl onto a graph paper sheet covered with a transparent plastic surface. Crawling was filmed at 60 fps with a digital camera (Sony ILCE-A6400) supported above the arena. The position of each point painted on the leech skin was tracked using DeepLabCut version 2.3.5 (He et al., 2016; Insafutdinov et al., 2016; Mathis et al., 2018; Nath et al., 2019). To this end, 338 frames randomly selected from 66 videos of 8 leeches were used for manually labeling the painted dots, and used for training a ResNet_50-based neural network for automating the detection.

To characterize crawling, steps were defined by the frames in which the algorithmic sum of the following values was at a minimum: 1) the whole length of the leech, 2) the velocity of the

most anterior dot, and 3) the velocity of the most posterior dot (Figure 5C). Steps where DeepLabCut failed to detect any of the nine points on the animal were discarded. After dividing the animal displacement into steps, we performed a quantitative analysis of the changes in the length of the animal sections (defined between each pair of points) over time. Specifically, the sections delimited by the painted points 4-5 and 5-6 were chosen since they include the range of ganglia considered in the electrophysiological studies (8-15). The length traces of each leech were filtered using a Gaussian filter (sigma of 0.25 s). For each step, the duration of the elongation and contraction stages within a section was calculated by using the maximum length as the boundary between these phases. The onset of elongation and the end of contraction were determined by detecting knee points, as described by Satopaa et al. (2011, Figure 5C).

Spike Sorting

Extracellular recordings were spike sorted using a custom-written algorithm which relies on a template matching-based method based on (Pouzat et al., 2002), incorporating a t-SNE model (Pedregosa et al., 2011; Van der Maaten and Hinton, 2008). Because spike sorting is sensitive to misclassification, the resulting output was manually curated to address whether a single cluster of waveforms was self-consistent with a single neuron (Hill et al., 2011). During manual curation, all clusters of putative spike events were evaluated. Clusters containing two well defined groups of waveforms were split and pairs of clusters with similar waveforms and temporally coordinated activity were merged. Clusters that had inconsistent waveforms and could not be split into clusters with well-defined waveforms were discarded. After this procedure, each cluster was considered a single motor unit.

To select for rhythmic units, autocorrelations were performed considering the first four cycles of the fictive behavior. Units whose autocorrelogram included at least 2 peaks with a correlation coefficient greater than 0.25 were considered rhythmic.

Data Processing

DE-3 spike times were derived from DP nerve recordings using the spike sorting algorithm mentioned above. DE-3 bursts were considered as such if they comprised at least 10 spikes with a mean firing frequency of 8 Hz, where the separation between two subsequent spikes occurred with a maximum separation of 0.5 seconds. Burst duration was calculated as the time difference between the last and first DE-3 spikes in each burst. Cycle period was calculated in two different ways: as the time difference between the last (end-to-end), or the first spikes (start-to-start) of subsequent DE-3 bursts, and is reported accordingly. Duty cycle was calculated as the ratio between burst duration and period. The mean firing frequency (mFF) of each burst was calculated as the number of spikes over the burst duration. The binned firing frequency (bFF) of DE-3, or any other unit, was obtained by binning the number of spikes along the recording using a 0.05 s or a 0.5 s interval, for Figure 2 and Figure 6, respectively. For cross-correlation analysis, the DE-3 bFF was filtered using a Gaussian filter (sigma of 150 ms).

For the cross-correlation between NS membrane potential and DE-3 firing frequency, the intracellular recording of NS was resampled to match the data rate of DE-3 bFF. To determine the amplitude of NS hyperpolarization, a baseline membrane potential was established using a Gaussian filter (sigma of 5 s) applied to the entire trace. The amplitude was calculated as the difference between the baseline value at the start of the DE-3 burst and the minimum membrane potential reached by NS during the corresponding burst (see Figure 2A).

When NS depolarization was implemented, the cycles including the onset or offset of the current pulse were excluded, and the traces were divided into three epochs: pre, test, and post. Control experiments were treated similarly.

When analyzing the activity of the units obtained by spike sorting, the maximum bFF value and relative half width were obtained from curves displaying bFF versus cycle-phase (time normalized to the period of each cycle). The relative half width was calculated as the width at half the maximum bFF value.

Data processing was performed using custom written Python scripts.

Statistical Analysis

All statistical analyses were performed using R (R Core Team, 2020). The goodness-of-fit for each model was analyzed using the DHARMa package. For every analysis, the structure of random factors was kept maximal whenever possible. The specific random factors considered in each case are detailed in Supplementary Tables 1 and 2.

To analyze the correlation between the amplitude of NS hyperpolarization and different *crawling* features (Figure 2D-G), the lmer function from the lmerTest package (Kuznetsova et al., 2017) was used to perform linear mixed models (LMM) with the experiment as a random factor.

To analyze the effect of NS depolarization on motoneuron activity, the data was analyzed using mixed-effects models with two fixed factors: epoch (pre, test, post) and treatment (control, depolarization). All models included motor units as a random factor. Each ganglion was also included as a random factor. The effect of NS depolarization was analyzed with the glmmTMB function from the glmmTMB package (Brooks et al., 2017) to perform a generalized linear

mixed model (GLMM) or with the lmer function to perform a LMM. For the GLMM, we used a student-t distribution (t_family) with the identity link or Gamma family with a log link as indicated in Supplementary Tables 1 and 2. The significance of a factor was determined with a likelihood-ratio test for the GLMM or an F-test for the LMM. This was done by comparing the model including the factor with a model dropping that factor. Pairwise simple contrasts were performed within the treatment factor and between the epoch factor using the *emmeans* package and the Tukey correction were applied to obtain the p values.

To analyze a possible temporal drift on *crawling* features we considered the data of control experiments and used mixed-effects models with epoch (pre, test, post) as a fixed factor and units as a random factor. Supplementary Tables 1 and 2 specifies the models used for each analysis.

Acknowledgments: The authors thank Drs. Violeta Medan, Graciela Kearney, Alejandro Cámera and Ronald Calabrese for highly valuable comments on the manuscript. We also thank M.Sc. Julieta Laurino for the highly valuable discussions on statistics. This work was supported by the following grants to LS: PICT 2016–2073 from Agencia Nacional de Promoción Científica y Tecnológica; UBACyT 20020150100179BA from Universidad of Buenos Aires and Human Frontier Science Program (RGP0060/2019).

REFERENCES

Alvarez, F.J., and Fyffe, R.E. 2007. The continuing case for the Renshaw cell. *J Physiol*. 584:31-45.

Arber, S., and R.M. Costa. 2018. Connecting neuronal circuits for movement. *Science*. 360:1403-1404.

Ashaber, M., Tomina, Y., Kassraian, P., Bushong, E. A., Kristan, W. B., Ellisman, M. H., & Wagenaar, D. A. (2021). Anatomy and activity patterns in a multifunctional motor neuron and its surrounding circuits. *eLife*, *10*, e61881. https://doi.org/10.7554/eLife.61881

Baader, A.P. 1997. Interneuronal and motor patterns during crawling behavior of semi-intact leeches. *J Exp Biol.* 200:1369-1381.

Baader, A.P., and W.B. Kristan. 1992. Monitoring neuronal activity during discrete behaviors: a crawling, swimming and shortening device for tethered leeches. *J. Neurosc. Meth.* 43:215-223.

Baca, S.M., A. Marín-Burgin, D.A. Wagenaar, and W.B. Kristan. 2008. Widespread inhibition proportional to excitation controls the gain of a leech behavioral circuit. *Neuron*. 57:276-289.

Barkan, C. L., & Zornik, E. (2019). Feedback to the future: motor neuron contributions to central pattern generator function. *The Journal of experimental biology*, 222(Pt 16), jeb193318. https://doi.org/10.1242/jeb.193318

Brooks, M.E., K. Kristensen, K.J. Van Benthem, A. Magnusson, C.W. Berg, A. Nielsen, H.J. Skaug, M. Machler, and B.M. Bolker. 2017. glmmTMB balances speed and flexibility among packages for zero-inflated generalized linear mixed modeling. *The R journal*. 9:378-400.

Calabrese RL & Marder E. (2024). Degenerate Neuronal and Circuit Mechanisms Important for Generating Rhythmic Motor Patterns. *Physiological Reviews*.

Callahan, R.A., R. Roberts, M. Sengupta, Y. Kimura, S.-i. Higashijima, and M.W. Bagnall. 2019. Spinal V2b neurons reveal a role for ipsilateral inhibition in speed control. *Elife*. 8:e47837.

Eisenhart, F.J., T.W. Cacciatore, and W.B. Kristan. 2000. A central pattern generator underlies crawling in the medicinal leech. *J Comp Physiol A*. 186:631-643.

El Manira, A. 2023. Modular circuit organization for speed control of locomotor movements. *Current Opinion in Neurobiology*. 82:102760.

Fan, R.J., A. Marín-Burgin, K.A. French, and W.O. Friesen. 2005. A dye mixture (Neurobiotin and Alexa 488) reveals extensive dye-coupling among neurons in leeches; physiology confirms the connections. *J Comp Physiol A*. 191:1157-1171.

Fushiki, A., Zwart, M. F., Kohsaka, H., Fetter, R. D., Cardona, A., and Nose, A. (2016). A circuit mechanism for the propagation of waves of muscle contraction in *Drosophila*. *eLife* 5:e13253.

Gal, J.-P.L., Dubuc, R. and Smarandache-Wellmann, C. 2017. Coordination of Rhythmic Movements. *In* Neurobiology of Motor Control. S.L.H.a.A. Büschges, editor. Wiley Blackwell. 305-332.

Grätsch, S., Büschges, A., & Dubuc, R. (2019). Descending control of locomotor circuits. *Current Opinion in Physiology*.

Grillner, S., and A. El Manira. 2020. Current Principles of Motor Control, with Special Reference to Vertebrate Locomotion. *Physiological Reviews*. 100:271-320.

He, K., X. Zhang, S. Ren, and J. Sun. 2016. Deep residual learning for image recognition. *In* Proceedings of the IEEE conference on computer vision and pattern recognition. 770-778.

Hennequin, G., Agnes, E. J., & Vogels, T. P. (2017). Inhibitory Plasticity: Balance, Control, and Codependence. *Annual review of neuroscience*, *40*, 557–579.

Hill, D. N., Mehta, S. B., and Kleinfeld, D. (2011). Quality metrics to accompany spike sorting of extracellular signals. *J. Neurosci*. 31, 8699–8705.

Insafutdinov, E., L. Pishchulin, B. Andres, M. Andriluka, and B. Schiele. 2016. Deepercut: A deeper, stronger, and faster multi-person pose estimation model. *In* Computer Vision–ECCV 2016: 14th European Conference, Amsterdam, The Netherlands, October 11-14, 2016, Proceedings, Part VI 14. Springer. 34-50.

Kearney, G., M. Radice, A. Sanchez Merlinsky, and L. Szczupak. 2022. Intersegmental Interactions Give Rise to a Global Network. *Front Neural Circuits*. 16.

Kiehn, O. 2016. Decoding the organization of spinal circuits that control locomotion. *Nat Rev Neurosci*. 17:224-238.

Kishore, S., M.W. Bagnall, and D.L. McLean. 2014. Systematic shifts in the balance of excitation and inhibition coordinate the activity of axial motor pools at different speeds of locomotion. *Journal of Neuroscience*. 34:14046-14054.

Kuznetsova, A., P.B. Brockhoff, and R.H.B. Christensen. 2017. lmerTest package: tests in linear mixed effects models. *Journal of statistical software*. 82.

Marín-Burgin, A., and L. Szczupak. 2003. Network interactions among sensory neurons. *J. Comp. Physiol. A*. 189:59-67.

Mason, A., and W.B. Kristan. 1982. Neuronal excitation, inhibition and modulation of leech longitudinal muscle. *J. Comp. Physiol.* 146:527-536.

Mathis, A., P. Mamidanna, K.M. Cury, T. Abe, V.N. Murthy, M.W. Mathis, and M. Bethge. 2018. DeepLabCut: markerless pose estimation of user-defined body parts with deep learning. *Nature neuroscience*. 21:1281-1289.

McLean, D.L., and K.J. Dougherty. 2015. Peeling back the layers of locomotor control in the spinal cord. *Curr Opin Neurobiol*. 33:63-70.

Muller, K.J., J.G. Nicholls, and G.S. Stent. 1981. Neurobiology of the leech. Cold Spring Harbor Laboratory, Cold Spring Harbor, NY.

Nath, T., A. Mathis, A.C. Chen, A. Patel, M. Bethge, and M.W. Mathis. 2019. Using DeepLabCut for 3D markerless pose estimation across species and behaviors. *Nature protocols*. 14:2152-2176.

Nishimaru, H., C.E. Restrepo, and O. Kiehn. 2006. Activity of Renshaw cells during locomotor-like rhythmic activity in the isolated spinal cord of neonatal mice. *J Neurosci*. 26:5320-5328.

Ort, C.A., W.B. Kristan, and G.S. Stent. 1974. Neuronal control of swimming in the medicinal leech. *J Comp Physiol A*. 94:121-154.

Parkis, M., X.-W. Dong, J. Feldman, and G. Funk. 1999. Concurrent inhibition and excitation of phrenic motoneurons during inspiration: phase-specific control of excitability. *Journal of Neuroscience*. 19:2368-2380.

Pedregosa, F., G. Varoquaux, A. Gramfort, V. Michel, B. Thirion, O. Grisel, M. Blondel, P. Prettenhofer, R. Weiss, and V. Dubourg. 2011. Scikit-learn: Machine learning in Python. *the Journal of machine Learning research*. 12:2825-2830.

Perez-Etchegoyen, C.B., R.J. Alvarez, M.J. Rodriguez, and L. Szczupak. 2011. The activity of leech motoneurons during motor patterns is regulated by intrinsic properties and synaptic inputs. *J Comp Physiol A Neuroethol Sens Neural Behav Physiol*. 198:239-251.

Petersen, P.C., M. Vestergaard, K.H. Jensen, and R.W. Berg. 2014. Premotor spinal network with balanced excitation and inhibition during motor patterns has high resilience to structural division. *Journal of Neuroscience*. 34:2774-2784.

Pouzat, C., O. Mazor, and G. Laurent. 2002. Using noise signature to optimize spike-sorting and to assess neuronal classification quality
. *J Neurosci Methods*. 122:43-57.

Puhl, J.G., and K.A. Mesce. 2008. Dopamine Activates the Motor Pattern for Crawling in the Medicinal Leech. *J. Neurosci.* 28:4192-4200.

Pulver, S. R., Bayley, T. G., Taylor, A. L., Berni, J., Bate, M., and Hedwig, B. (2015). Imaging fictive locomotor patterns in larval *Drosophila*. *J. Neurophysiol*. 114, 2564–2577. doi: 10.1152/jn.00731.2015

Rela, L., and L. Szczupak. 2003. Coactivation of motoneurons regulated by a network combining electrical and chemical synapses. *J. Neurosci.* 23:682-692.

Rela, L., and L. Szczupak. 2007. In situ characterization of a rectifying electrical junction. *J. Neurophysiol.* 97:1405-1412.

Rela, L., S.M. Yang, and L. Szczupak. 2009. Calcium spikes in a leech nonspiking neuron. *J. Comp. Physiol.* 195:139-150.

Rodriguez, M.J., R.J. Alvarez, and L. Szczupak. 2012. Effect of a nonspiking neuron on motor patterns of the leech. *J Neurophysiol*. 107:1917-1924.

Rodriguez, M.J., C.B. Perez-Etchegoyen, and L. Szczupak. 2009. Premotor nonspiking neurons regulate coupling among motoneurons that innervate overlapping muscle fiber populations *J. Comp. Physiol. A*. 195:1432-1351.

Rotstein, H.G., E. Schneider, and L. Szczupak. 2017. Feedback Signal from Motoneurons Influences a Rhythmic Pattern Generator. *J Neurosci*. 37:9149-9159.

Satopaa, V., Albrecht, J., Irwin, D., & Raghavan, B. 2011. Finding a "Kneedle" in a Haystack: Detecting Knee Points in System Behavior. In 2011 31st international conference on distributed computing systems workshops (pp. 166-171). IEEE.

Sengupta, M., and M.W. Bagnall. 2023. Spinal interneurons: diversity and connectivity in motor control. *Annual Review of Neuroscience*. 46:79-99.

Stern-Tomlinson, W., M.P. Nusbaum, L.E. Perez, and W.B. Kristan. 1986. A kinematic study of crawling behavior in the leech, hirudo medicinalis. *J. Comp. Physiol A*. 158:593-603.

Szczupak, L. 2014. Recurrent inhibition in motor systems, a comparative analysis. *J Physiol Paris*. 108:148-154.

Van der Maaten, L., and G. Hinton. 2008. Visualizing data using t-SNE. *Journal of machine learning research*. 9.

Wadepuhl, M. 1989. Depression of excitatory motoneurons by a single neuron in the leech central nervous system. *J Exp Biol.* 143:509-527.

Wagenaar, D.A. 2015. A classic model animal in the 21st century: recent lessons from the leech nervous system. *J Exp Biol*. 218:3353-3359.

Zhen, M., and A.D. Samuel. 2015. C. elegans locomotion: small circuits, complex functions. *Curr Opin Neurobiol*. 33:117-126.

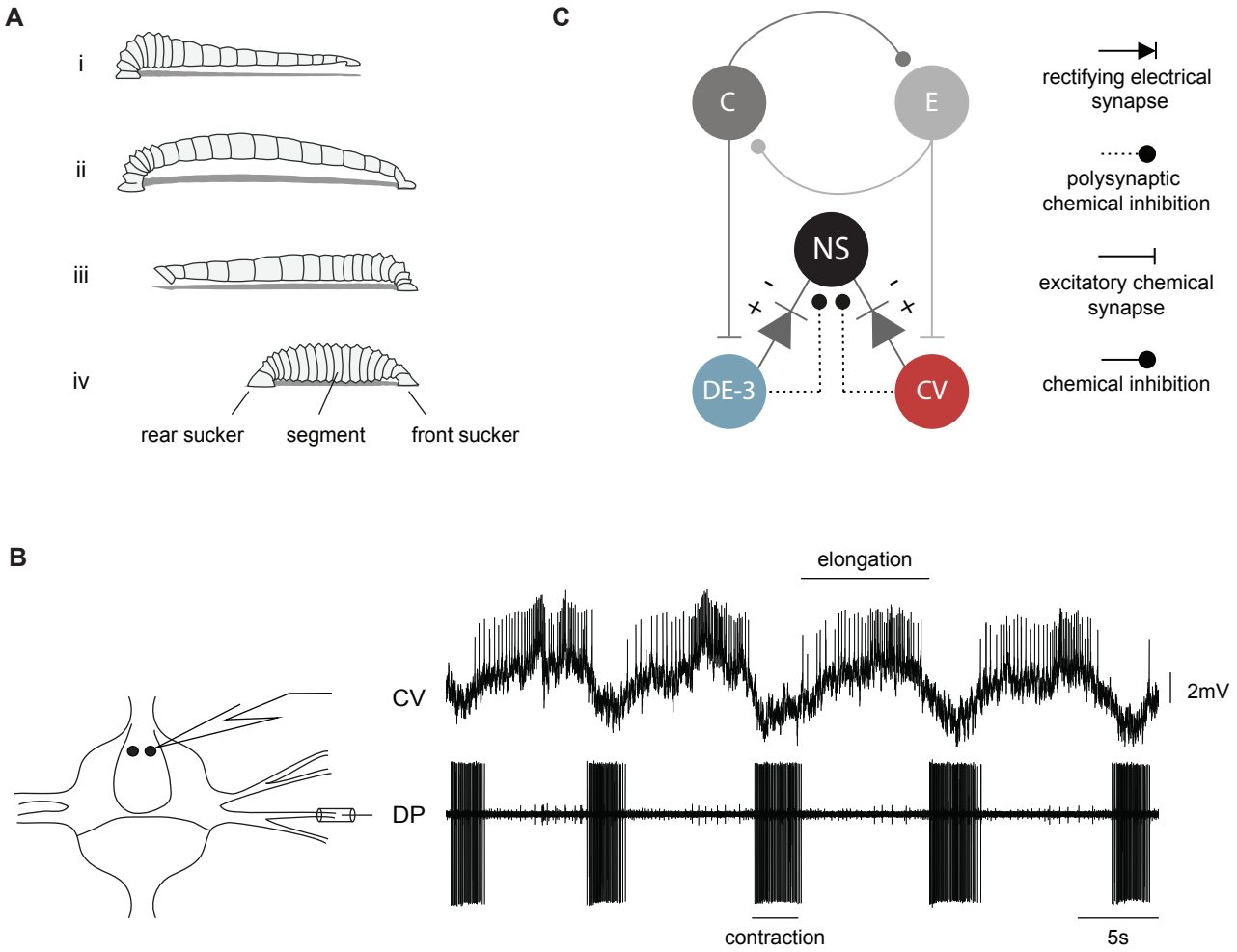

Figure 1. The crawling motor pattern. A. Schematic description of a leech crawling step that results from coordinated waves of elongation (i-ii) and contraction (iii-iv) phases, anchored on front and rear suckers. **B.** Intracellular recording of CV and extracellular recording of DE-3 (in DP nerve) motoneurons during a dopamine-induced crawling episode in an isolated midbody ganglion. Recording diagram on the left. **C.** Putative neuronal circuitry underlying crawling and the recurrent inhibitory circuit in a midbody ganglion. Units C and E correspond to contraction and elongation units of the segmental oscillator, respectively. DE-3 and CV are examples of motoneurons involved in each phase. NS neuron is connected to DE-3 and CV (Rela and Szczupak, 2003; Rodriguez et al., 2009) through chemical and electrical synapses; the + and - symbols indicate the polarity at which the rectifying synapse conducts.

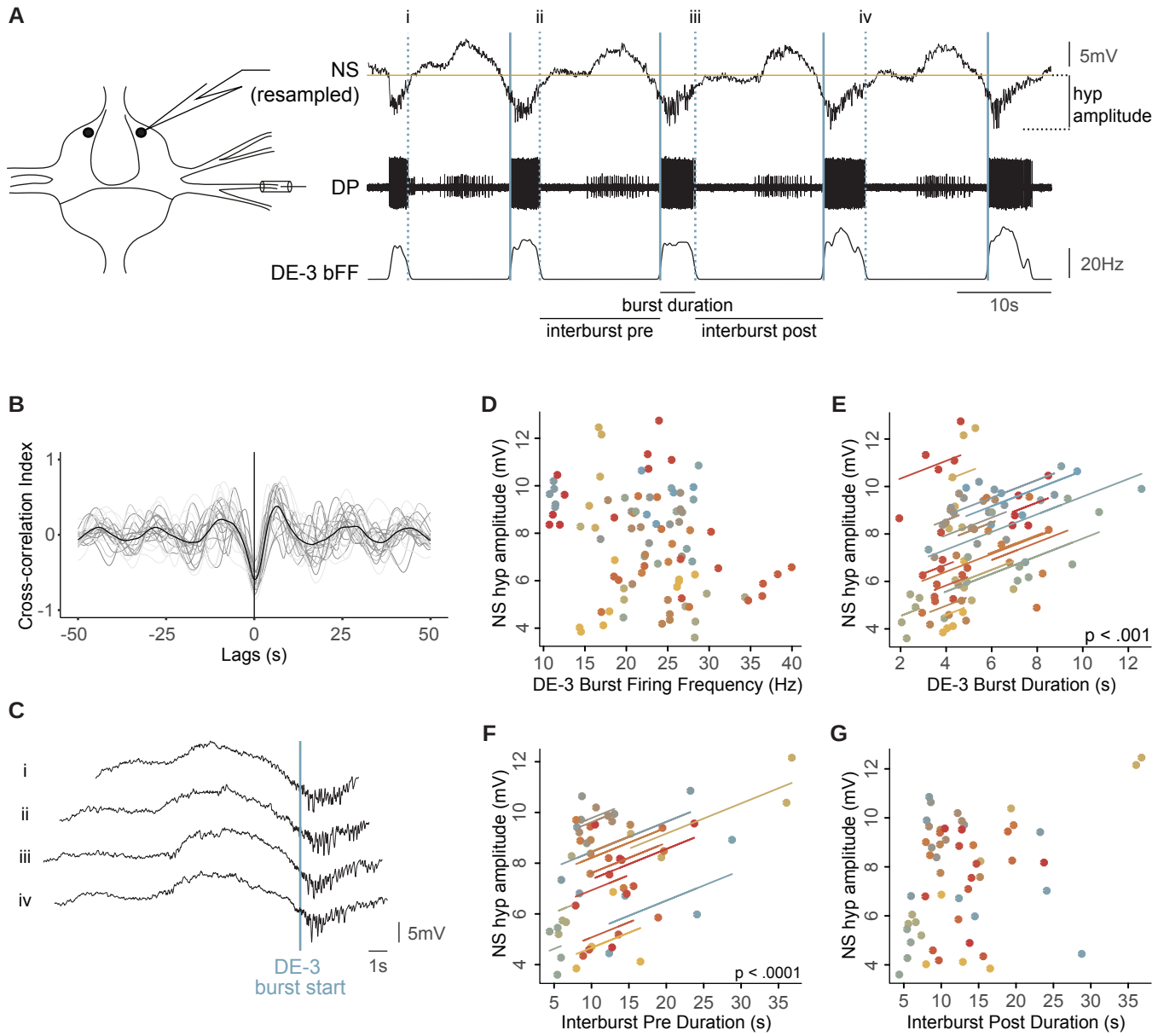

Figure 2. NS activity correlates with the crawling motor pattern. A. NS intracellular recording, DP extracellular recording and DE-3 binned firing frequency (bFF) during a crawling episode. NS recording was resampled to match the data rate of DE-3 bFF. Recording diagram on the left. The blue vertical line marks the beginning and the blue dotted line the end of each DE-3 burst. Different crawling features and NS hyperpolarization amplitude (NS hyp amplitude) are indicated. **B.** Cross-correlograms of the DE-3 bFF curves and NS resampled traces. Each gray trace corresponds to an individual experiment. The black curve corresponds to the mean cross-correlogram. (n = 23 crawling episodes containing 5 cycles, obtained in 23 ganglia from 18 leeches). **C.** Successive cycles of the NS recording shown in panel A, segmented at the times indicated by the dotted lines and aligned by the times indicated by solid blue lines indicated in A. **D.** NS hyperpolarization amplitude as a function of DE-3 Burst FF. **E.** Like in D, as a function of DE-3 burst duration. **F.** Like in D, as a function of interburst lag preceding DE-3 bursts. **G.** Like in D, as a function of the interburst lag after DE-3 bursts. For D-G, n = 19 crawling episodes, with 5 cycles each. In D to G, the correlation was tested using linear mixed-effects models, contemplating different experiments as a random variable. In D and G, $p>0.05$, and in E and F, $p<0.05$. The lines correspond to regressions obtained from the linear mixed-effects model. The coefficients were 0.374 ± 0.089 mv/s for E and 0.122 ± 0.034 mv/s for F.

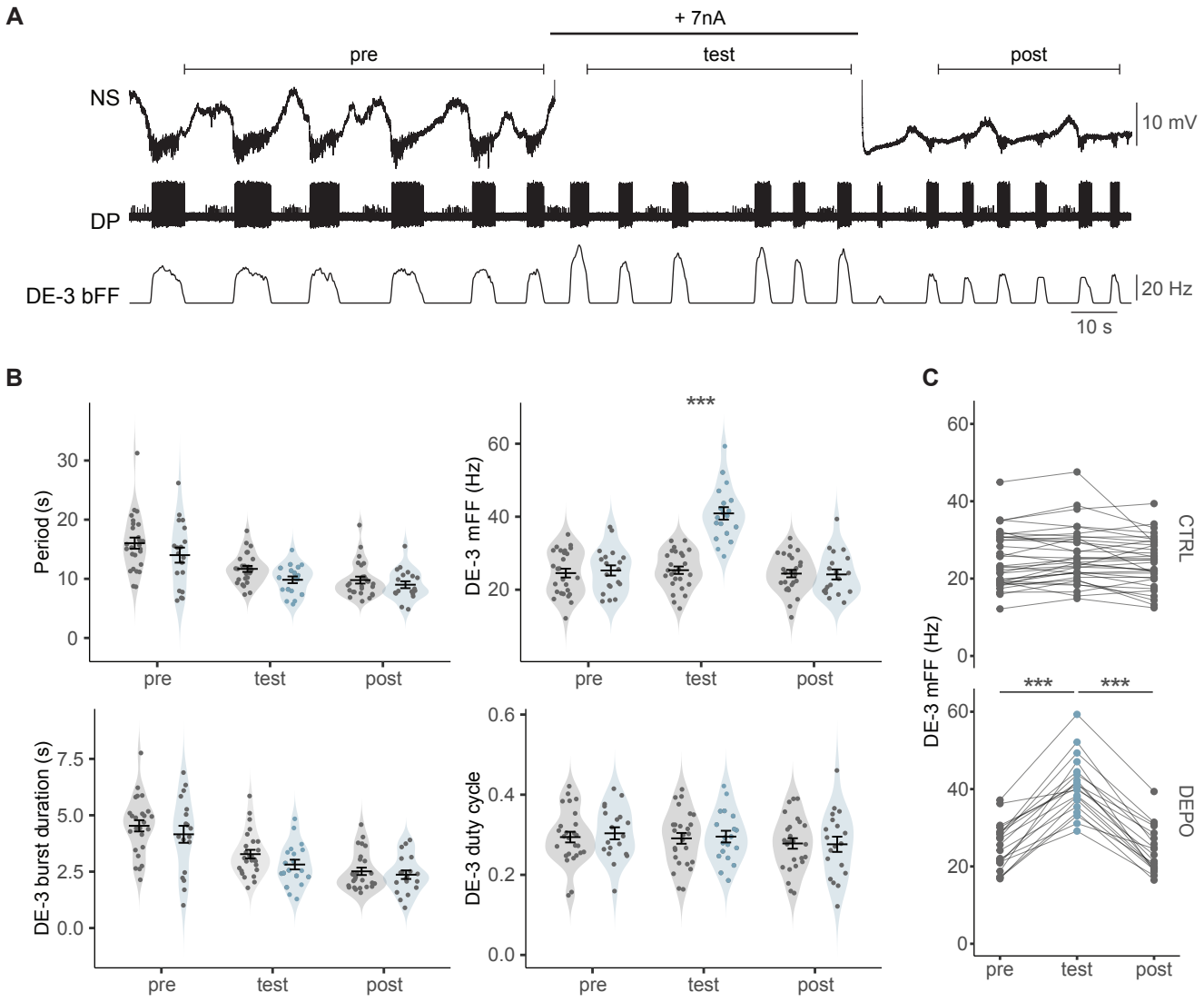

Figure 3. Effect of NS on crawling. A. Intracellular NS and extracellular DP recordings during a dopamine-induced crawling episode. A +7 nA pulse was injected in NS at the time indicated by the thick line. Segments above the recordings mark three epochs: previous (pre), during (test) and after (post) the pulse. **B.** Crawling period (end-to-end), DE-3 mFF, burst duration and duty cycle for cycles in the three epochs marked in A, for control experiments where no current was injected in NS (gray violins, n= 120 cycles from 26 episodes in 26 ganglia from 16 leeches) and for experiments where NS was depolarized (light blue violins, n= 92 cycles from 19 episodes in 19 ganglia from 15 leeches); each point corresponds to the mean value during the epoch for each individual experiment. Bars provide the mean ± SEM. *** $p<0.001$ (interaction between epoch and treatment factors). **C.** Mean DE-3 mFF for the three epochs from each individual experiment for control (CTRL) and depolarizing (DEPO) tests. Lines link dots that correspond to each individual experiment. *** $p<0.001$ (pairwise simple contrasts, Δ pre-test = -15.591 ± 1.037 Hz and Δ test-post = 16.648 ± 0.919 Hz).

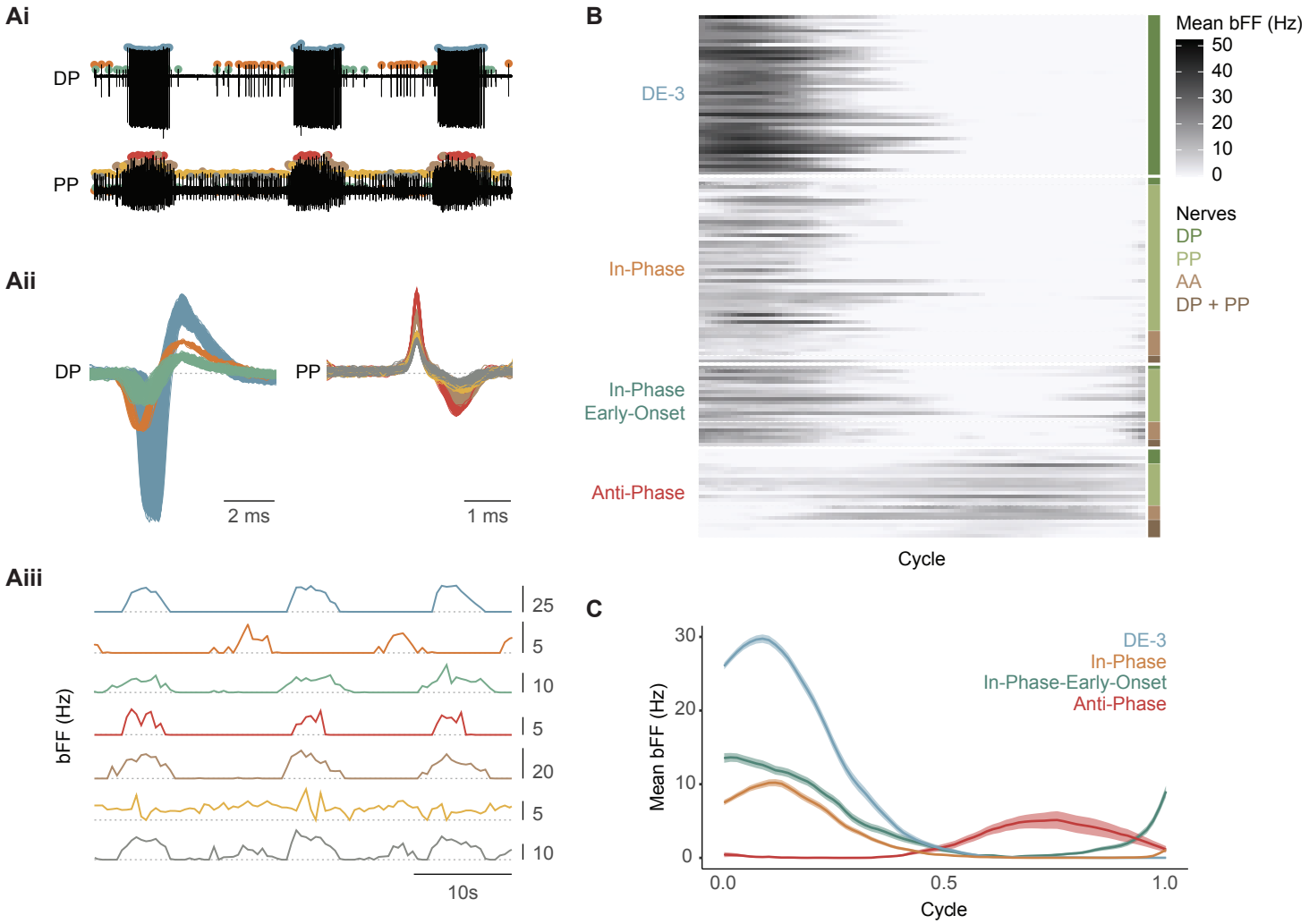

Figure 4. Profile of motoneuron activity during crawling. A.i. Representative example of a spike sorting analysis implemented in paired extracellular recordings of DP and PP nerves during a crawling episode. Each color dot singles out a distinct active unit along the recordings. **A.ii.** Spikes waveforms corresponding to spikes detected in the DP and PP nerves in Ai. **A.iii.** bFF calculated for each unit identified in A. The horizontal dotted lines indicate bFF = 0 Hz. Scales on the right are in Hz. **B.** Raster plot showing mean bFF along a cycle, set from the first spike of a DE-3 burst to the first spike in the next burst, obtained from 147 rhythmic units identified in DP, PP and AA nerves (n = 46 ganglia in 24 animals). The values are the mean of 4 crawling cycles for each unit. The units were classified into four groups, indicated on the left. The nerves from which the motoneuron activity was recorded are indicated on the right. The gray scale on the right indicates the bFF value in Hz. **C.** Mean bFF for all the units included in each group. The shaded area represents the standard error of the mean.

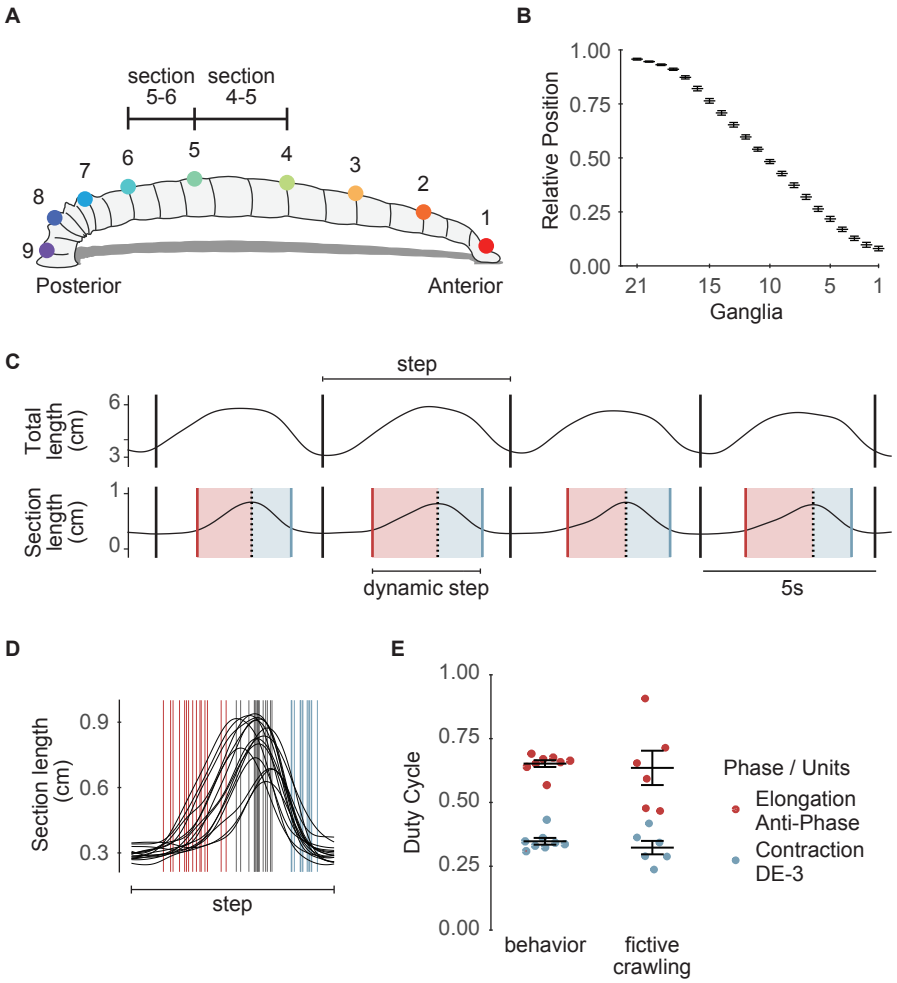

Figure 5. Analysis of leech crawling. A. Schematic representation of a leech with nine points as painted on their dorsal midline. The sections between points 4-5 and 5-6 comprise ganglia 8-15 that were used for the electrophysiological analysis. **B.** Relative position of midbody ganglia 1–21. Mean and standard error of the mean are shown (n = 3) (Kearney et al. 2022). **C.** Representative example of the changes in total length and section 4-5 of a leech during four steps as the animal was crawling. The limits of each step are indicated by black vertical lines (see Materials and Methods); red and blue vertical lines mark the start of elongation and the end of contraction, respectively; black dashed vertical lines indicate the maximal section length. Light red and blue shades indicate elongation and contraction phases, respectively. **D.** Superimposed length curves of a section across random multiple steps (n= 15 of 76 total steps for this animal) of one leech. **E.** Duty Cycle of the elongation and contraction phases measured in crawling behavior or in fictive crawling. Behavioral variables were calculated as the duration of each phase relative to the sum of elongation and contraction phases (dynamic step in C), excluding isometric phases. Points represent the mean for each leech, while bars and lines indicate the mean ± SEM across all leeches (n = 249 steps from 8 leeches). For the Duty Cycle of DE-3 and Anti-Phase units, points correspond to the mean for each ganglion, with bars and lines showing the mean ± SEM across all ganglia (n = 4 cycles for each DE-3 or Anti-Phase motoneuron, 6 ganglia, 6 leeches).

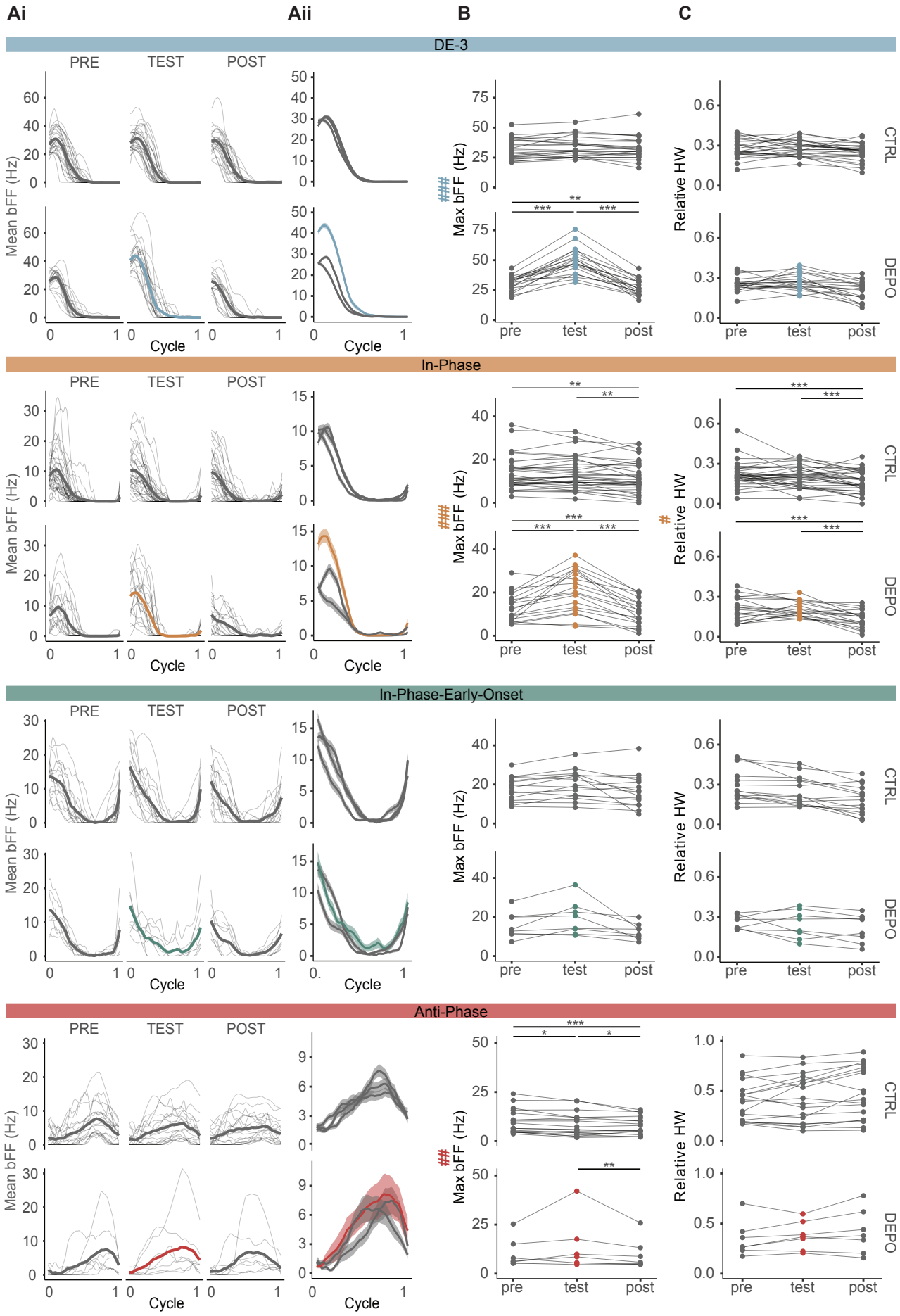
Ai
Aii
B
C
DE-3
PRE
TEST
POST
Mean bFF (Hz)
Cycle
Max bFF (Hz)
Relative HW
pre
test
post
CTRL
DEPO
In-Phase
In-Phase-Early-Onset
Anti-Phase

Figure 6. Effect of NS on the different phases of crawling. A.i. Mean bFF along cycles in pre, test, and post epochs for each unit within the four groups described in Figure 4. For each unit type the upper line of graphs presents control experiments, where no current was injected in NS, and the bottom line, depolarization experiments, where 5-7 nA current steps were injected in NS during the test epoch. Thin lines show the mean bFF (including 4 - 6 cycles) for each experiment, and thick lines show the overall mean. **A.ii.** Superimposition of the overall bFF mean of the three epochs. The shaded area presents the standard error of the mean. **B** & **C.** Maximum bFF (Max bFF) and Relative Half Width (Relative HW) measured in each individual unit. A-C are plotted for each of the four groups of units indicated. Lines connect the mean values across each epoch within the same experiment. Mixed-effects models with two fixed factors were performed; on the left of the B and C panel, # indicates a significant interaction between treatment and epoch factors; * indicates significant differences for pairwise simple contrasts between epochs, within each treatment. *, ** and *** (or #) indicate $p<0.05$, $p<0.01$ and $p<0.001$, respectively. Supplementary Table 2 describes the statistical models performed. For DE-3, n= 26 control and 20 depolarization ganglia, from 46 ganglia; for In-Phase, n= 38 units for control and 21 units for depolarization, from 30 ganglia; for Anti-Phase, n= 18 units for control and 7 units for depolarization experiments, from 22 ganglia; and for In-Phase-Early-Onset, n= 15 units for control and 8 units for depolarization experiments, from 23 ganglia.

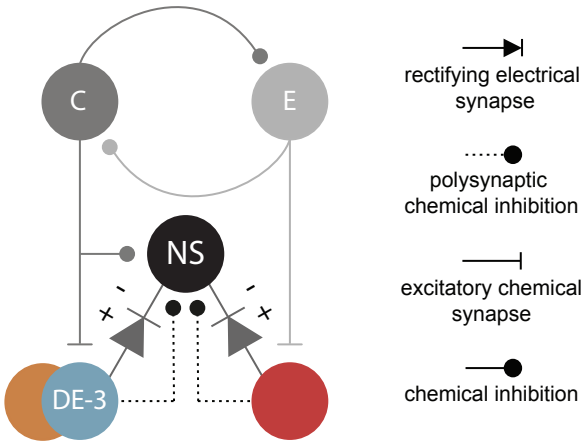

Figure 7. NS in the crawling circuitry. Putative neuronal circuitry as described in Figure 1C, including the connection between the oscillatory circuit and NS. The colors used here match those identifying the units in Figures 4 and 6.

Effect of NS depolarization on *crawling* features. (n units = 26 ctrl, 19 depo / n leeches = 16 ctrl, 15 depo).					
Variable	Model, random effects	Significance of factor interactions	Pairwise simple contrasts		
			Comparison	Ratio	p value
DE-3 FF	LMM intercept - unit slope - epoch	<.0001	ctrl test / pre post / pre post / test depo test / pre post / pre post / test	 1.04 1 0.96 1.62 0.96 0.59	 0.6345 0.9815 0.4654 <.0001 0.3909 <.0001
DE-3 burst duration	GLMM - Gamma family, log link intercept - unit slope - epoch	0.3077	-	-	-
period	GLMM - Gamma family, log link intercept - units	0.2107	-	-	-
DE-3 duty cycle	LMM intercept - unit slope - epoch	0.8309	-	-	-
Effect of temporal drift on *crawling* features. (n units = 26 ctrl, 19 depo / n leeches = 16 ctrl, 15 depo)					
Variable	Model, random effects	Significance of factor	Fixed effects		
			Epoch	Estimate	p value
DE-3 burst duration	GLMM - Gamma family, log link intercept - unit	<.0001	pre (intercept) test post	4.40 3.16 2.44	<.0001 <.0001 <.0001
period	GLMM - Gamma family, log link intercept - unit	<.0001	pre (intercept) test post	15.45 11.45 9.47	<.0001 <.0001 <.0001
DE-3 duty cycle	LMM intercept - unit	0.1623	-	-	-

Supplementary Table 1. Statistical Models Performed for the Effect Analysis of NS depolarization on *crawling* features and DE-3 activity during the fictive behavior. For each analyzed variable, it is specified whether a Linear Mixed Model (LMM) or a Generalized Linear Mixed Model (GLMM) was used, along with the structure of random factors. For GLMMs, the corresponding distribution and link function are also provided. Significance, p-values, and estimated ratios or values are reported for each model.

Variable	Model, random effects	Significance of factor interactions	Pairwise simple contrasts		
			Comparison	Ratio	p value
Effect of NS depolarization on motoneuron activity during *crawling*.					
DE-3 (n units = 26 ctrl, 20 depo / n cycles = 110 ctrl, 99 depo / n leeches = 16 ctrl, 16 depo)					
Max FF	LMM intercept - unit slope - treatment and epoch	<.0001	ctrl test / pre post / pre post / test depo test / pre post / pre post / test	 1.04 1 0.96 1.59 0.89 0.56	 0.5512 0.9995 0.5406 <.0001 0.0066 <.0001
Rel HW	LMM intercept - unit slope - treatment and epoch	0.1596	-	-	-
In-Phase (n units = 34 ctrl, 19 depo / n cycles = 149 ctrl, 93 depo / n experiments = 17 ctrl, 11 depo / n leeches = 13 ctrl, 8 depo)					
Max FF	GLMM - t_family, identity link intercept - experiment/unit	<.0001	ctrl test / pre post / pre post / test depo test / pre post / pre post / test	 1.01 0.92 0.91 1.52 0.86 0.56	 0.9628 0.0046 0.0014 <.0001 0.0005 <.0001
Rel HW	GLMM - t_family, identity link intercept - experiment/unit	0.01492	ctrl test / pre post / pre post / test depo test / pre post / pre post / test	 0.93 0.78 0.84 0.99 0.60 0.61	 0.1788 <.0001 0.0007 0.9840 <.0001 <.0001
Anti-Phase (n units = 18 ctrl, 7 depo / n cycles = 78 ctrl, 34 depo / n experiments = 15 ctrl, 7 depo / n leeches = 12 ctrl, 7 depo)					
Max FF	GLMM - t_family, identity link intercept - experiment/unit	0.00148	ctrl test / pre post / pre post / test depo test / pre post / pre post / test	 0.91 0.82 0.90 1.10 0.94 0.85	 0.0104 <.0001 0.0180 0.0505 0.4132 0.0025
Rel HW	GLMM - t_family, identity link intercept - experiment/unit	0.9791	-	-	-
In-Phase-Early-Onset (n units = 15 ctrl, 8 depo / n cycles = 66 ctrl, 45 depo / n experiments = 12 ctrl, 5 depo / n leeches = 11 ctrl, 5 depo)					
Max FF	LMM intercept - experiment/unit	0.0891	-	-	-
Rel HW	GLMM - t_family, identity link intercept - experiment/unit	0.173	-	-	-

Supplementary Table 2. Statistical Models Performed for the Effect Analysis of NS depolarization on different groups of units activity during *crawling*. For each analyzed variable, it is specified whether a Linear Mixed Model (LMM) or a Generalized Linear Mixed Model (GLMM) was used, along with the structure of random factors. For GLMMs, the corresponding distribution and link function are also provided. Significance, p-values, and estimated ratios are reported for each model.